Hindawi
Advances in Civil Engineering
Volume 2022, Article ID 7548284, 8 pages
https://doi.org/10.1155/2022/7548284

*Research Article*

# Experimental Study on Warm Permafrost Dynamic Characteristics under Cyclic Loading in the Cold Region

**Liwei Song,[1] Junfang Liu ,[2] Yan Jin,[2] Chi Li,[2] and Songbao Cai[1]**

[1]*Technology Center, China Construction Sixth Engineering Bureau Co., Ltd, Tianjin, China*
[2]*Civil Engineering College, Inner Mongolia University of Technology, Hohhot, China*

Correspondence should be addressed to Junfang Liu; 574356727@qq.com

Received 5 May 2022; Revised 12 August 2022; Accepted 13 August 2022; Published 13 September 2022

Academic Editor: Luigi Fenu



With the rapid development of infrastructure construction, some places have to face the problem of highway foundation disease, especially for the highway built on warm permafrost in cold region. In order to analyze the influence of confining pressure and vehicle load to the warm permafrost, the dynamic triaxial tests were conducted on the frozen soil extracted from highway in Yakeshi City. While the load frequency is 6 Hz and the test temperature is −1.5°C, we changed the confining pressure and axial stress amplitude, respectively, and then gained the deviator stress-strain curves. The test results show that the shape of deviator stress-strain curve is related to the deviator stress amplitude. When $\sigma_3$ = 25 kPa and $|\sigma_1-\sigma_3|_{max}$ = 75 kPa, the hysteretic loops approximately appear rectangular and the dynamic modulus increases with loading time increasing for the compression effect. The specimen did not fail when the test stopped, and its hysteretic loop is stable. When $\sigma_3$ = 20 kPa and $|\sigma_1-\sigma_3|_{max}$ = 100 kPa, the hysteretic loops become smoother and appear oval. The test stopped while the axial strain reached 5% after loading 1279 times, and the dynamic modulus decreases with loading time increasing. When $\sigma_3$ = 30 kPa and $|\sigma_1-\sigma_3|_{max}$ = 115 kPa, the test stopped just after the 154$^{th}$ loop, and the hysteretic loop area linearly decreased with increasing loading time. The research conclusions in this article have numerous reference values for the highway design, construction, and operation built on the warm permafrost.

## 1. Introduction

With large-scale construction of infrastructure in China, the highway mileage is largely increasing in the northeast region. For the cold climate, the subgrade works in a poor condition, and the problems of seasonal frozen soil and permafrost need to be solved. Permafrost', especially for the warm permafrost, accumulative plastic deformation is obvious under traffic loading that causes road settlement.

This study reveals the dynamic characteristics of warm permafrost under cyclic loading with different confining pressure and dynamic stress amplitude, and it can provide technical reference for the highway design, construction, and operation in the future that built on the warm permafrost. It is also important to avoid highway foundation disease caused by excessive vehicle load.

The warm permafrost is the frozen soil that the temperature is between −1.5°C and 0.0°C, so it is also called permafrost in phase change zone. The warm permafrost is sensitive to the temperature change, and its mechanical property is more complicated than other permafrost [1].

Xu et al. [2] studied the dynamic stress-strain relationship for frozen soil and presented the relation between the damping ratio and experimental temperature, confining pressure, water content, and vibratory frequency. The main influencing factors to the damping ratio are experimental temperature, confining pressure, and frequency.

Zhao et al. [3] tested the frozen soil parameters including dynamic elastic modulus and dynamic damping ratio and found variation laws of dynamic mechanics parameters of frozen silty clay and fine sand are the same. The dynamic elastic modulus of frozen soil increases with increment of frequency.

Dynamic triaxial tests are carried out on frozen clay sampled from the Qinhai-Tibet railway under different temperature and confining pressure [4]. The frozen soil

dynamic strength linearly decreases with the increase in logarithmic cyclic number.

Gao et al. [5] studied the dynamic characteristics of warm and ice-rich frozen soil. The dynamic modulus decreases as the dynamic strain increases when the confining pressure is larger than 0.5 MPa, while the dynamic modulus increases at first and then decreases as the dynamic strain increases when the confining pressure is below 0.5 MPa.

The dynamic modulus of frozen soil is affected by confining pressure, frequency, temperature, and water content, and the damping ratio decreases as frequency increases and temperature decreases [6].

The dynamic properties of frozen clay are studied by hysteresis curves, and the result showed the soil stiffness increases, while the viscosity, degree of microscopic damage, residual strain, and energy dissipation decrease with the decreasing temperature and increasing vibration frequency when the temperature is −0.5°C to 4°C and the vibration frequency is 1–10 Hz [7].

The dynamic strength characteristics of frozen silty clay was studied using triaxial cycle tests when the confining pressures vary between 0.3 MPa and 16 MPa and the temperature between −4°C and −6°C. The dynamic strength depended not only on the number of vibration and confining pressures but also on loss of energy resulted from cyclic loading [8].

The dynamic properties of the frozen soil were studied by experiments [9, 10] in recent years.

Xue et al. [11, 12] explored the influence mechanism of gas pressure on coal deformation, failure, and energy evolution and conduced two-phase flow simulation by the numerical analysis method.

The warm frozen soil mechanical characteristics were studied and gained lots of important conclusions [9, 13–21].

Some other scholars [22–30] studied the mechanical properties of warm permafrost by different methods and gained lots of useful conclusions to guide design and construction.

Yakeshi City is located in west of the Greater Khingan Mountain's median ridge in the northeast of Inner Mongolia Autonomous Region, and the reference geological information reveals there is extensive warm permafrost in this area. In order to investigate the dynamic properties of frozen subgrade in this area, the frozen triaxial tests were conducted on the remoulded soil.

## 2. The Testing Instrument, Specimen, and Testing Process

*2.1. The Testing Instrument and Specimen.* All the tests were conducted on the STX-100 dynamic triaxial tester made by American GCTS Company, as shown in the Figure 1. The maximum axial pressure is 25 kN, the maximum frequency is 10 Hz, the maximum hydraulic cylinder stroke length is 50 mm, and the maximal confining pressure is 2 MPa. The tester connects to a homothermal liquid circulation system and maintains a constant temperature by cooling liquid circulator. The liquid temperature can be changed from −50°C to 200°C in this system.

The specimens are remoduled by the soil extracted from highway subgrade in Yakeshi City, which is sifted by 2 mm geotechnical screen. The sifted soil dense is 1.74 g/cm$^3$; then, the soil is remoduled to specimens with 16.5% water content. The radius of specimen is 38 mm, while its height is 76 mm.

The specimen is installed in the freezing chamber in the tester and was kept at −1.5°C for 12 hours; then, uniformly start loading on the specimen.

*2.2. Loading Process.* The cyclic loading is loaded on the top of frozen soil specimen, and the confining pressures are 25 kPa, 20 kPa, and 30 kPa, while the corresponding axial pressure is 25 kPa, 40 kPa, and 42.5 kPa respectively. First, linearly load axial pressure and confining pressure, then the both pressures remain stationary for consolidation, and then load the cyclic loading on the specimen. The loading process is shown in Figure 2.

*2.3. Test Parameters.* The frozen triaxial test parameters such as temperature, frequency, confining pressure, and dynamic cyclic stress amplitude are listed in Table 1.

According to GB/T 50269-2015 [31], stop testing when the specimen axial strain reaches 5% or the cyclic number reaches 50000 whose axial strain still not reaches 5%.

## 3. Results and Discussion

*3.1. The Test Result When $\sigma_3 = 25$ kPa, $|\sigma_1 - \sigma_3|_{max} = 75$ kPa.* The deviator stress–axial dynamic strain curves are shown in Figure 3 for the $100^{th}$–$110^{th}$, $1000^{th}$–$1010^{th}$, $10000^{th}$–$10010^{th}$, $30000^{th}$–$30010^{th}$, and $49990^{th}$–$50000^{th}$ hysteretic loop, respectively. The density degree of hysteretic loop increases with loading time increasing, and the hysteretic loop center moves to the right gradually, but the maximal axial strain is only 0.46% which does not reach 5% when the test stopped. The hysteretic loop is stable and the specimen did not fail in the test.

The hysteretic loops of specimen appear rectangular, and the specimen has elastic and strain hysteretic properties during loading and unloading processes. In the primary phase, the dynamic load increased gradually and the pores were compressed, so the plastic deformation increased. With increasing cyclic loading time, the plastic deformation increment converged gradually, and the specimen maintains stability in the test.

The area of hysteretic loops was gained from the $1000^{th}$, $5000^{th}$, $10000^{th}$, $25000^{th}$, and $5000^{th}$ curves, and it decreases linearly with increasing loading time, as shown in Figure 4.

The hysteretic loop area can be calculated by the following equation:

$$S = -3.73 \times 10^{-8} N + 0.01384, \quad (1)$$

where $N$ is the loading time, and $S$ is the hysteretic loop area. The correlation coefficient is above 0.85 for equation (1).

According to [12], the dynamic modulus $E_d$ is calculated according to the following equation and Figure 5.


Figure 1: The STX-100 dynamic triaxial tester.

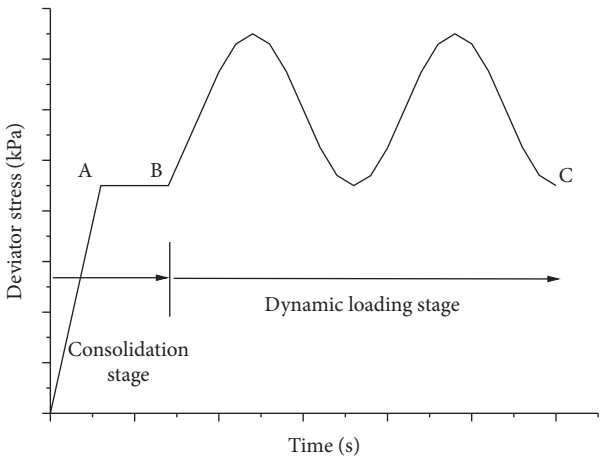


Figure 2: Loading process of the cyclic triaxial test.

Table 1: Test parameters.

| Temperature/°C | Load frequency/Hz | Confining pressure/kPa | Cyclic stress amplitude/kPa |
|---|---|---|---|
| −1.5 | 6 | 25 | 25 |
| −1.5 | 6 | 20 | 40 |
| −1.5 | 6 | 30 | 42.5 |

$$E_d = \frac{\sigma_d}{\varepsilon_d}, \tag{2}$$

where $\sigma_d$ is the dynamic axial stress, and $\varepsilon_d$ is the dynamic axial strain.

The dynamic damping coefficient $\lambda$ was calculated by the following equation.

$$\lambda = \frac{1}{\pi}\frac{S_{\text{shade}}}{S_{\Delta ABC}}, \tag{3}$$

where $S_{\text{shade}}$ is the shade area, and $S_{\Delta ABC}$ is the area of $\Delta ABC$ in Figure 5.

From the 1000th, 5000th, 10000th, 25000th, and 50000th hysteretic loop curves, the dynamic modulus and damping ratio of warm permafrost were calculated, and the results are listed in Table 2.

The dynamic properties of warm permafrost are basically stable when the confining pressure is 25 kPa and the axial pressure is not more than 75 kPa. With the increasing loading time, the specimen is compressed to be stiffer, and its dynamic modulus slightly rises while the damping ratio drops slightly.

*3.2. The Test Result When $\sigma_3 = 20$ kPa, $|\sigma_1 - \sigma_3|_{max} = 100$ kPa.* The deviator stress–axial dynamic strain curves are shown in Figure 6 for the 400th–410th, 800th–810th, and 1269th–1279th hysteretic loop, respectively. When the cyclic loading time is 1279, the axial strain reaches 5%, and then, the test stopped.

The hysteretic loop curves are approximately oval. With increasing loading time, the hysteretic loop center moves to the right faster, which means the axial strain increases faster than the previous test. The hysteretic loops are more intensive with increasing loading time.

After extracting the 400th, 600th, 800th, 1000th, and 1200th hysteretic loop curves, the relationship of hysteretic loop area and loading times was gained, as shown in Figure 7.

The hysteretic loop area $S$ can be calculated by the following equation:

$$S = -6 \times 10^{-5} N + 0.0598, \tag{4}$$

where $N$ is the loading time. The correlation coefficient is above 0.92 for equation (4).

The dynamic modulus and damping ratio under different loading times are listed in Table 3.

The hysteretic area linearly decreases with loading time basically. For the accumulation of damage in the specimen, the dynamic modulus decreased with increasing loading time basically in the test.

*3.3. The Test Result When $\sigma_3 = 30$ kPa, $|\sigma_1 - \sigma_3|_{max} = 115$ kPa.* First, both the axial pressure and confining pressure linearly increased until the values reached 30 kPa and then gradually loaded the axial cyclic loading with a 42.5 kPa amplitude until the axial strain reached 5%.

Extracted the 40th–50th, 90th–100th, and 140th–154th hysteretic loops, as shown in Figure 8; the hysteretic loops presented to ovals in the loading and uploading processes. The hysteretic loop appears with viscoelastic properties with high deviator stress for the warm permafrost. With increasing loading time, the hysteretic loop center moves to the bigger strain direction, and plastic deformation accumulated gradually until the axial strain reached 5%. The plastic deformation increment is smaller and smaller that is manifested by the hysteretic loop density in Figure 8.

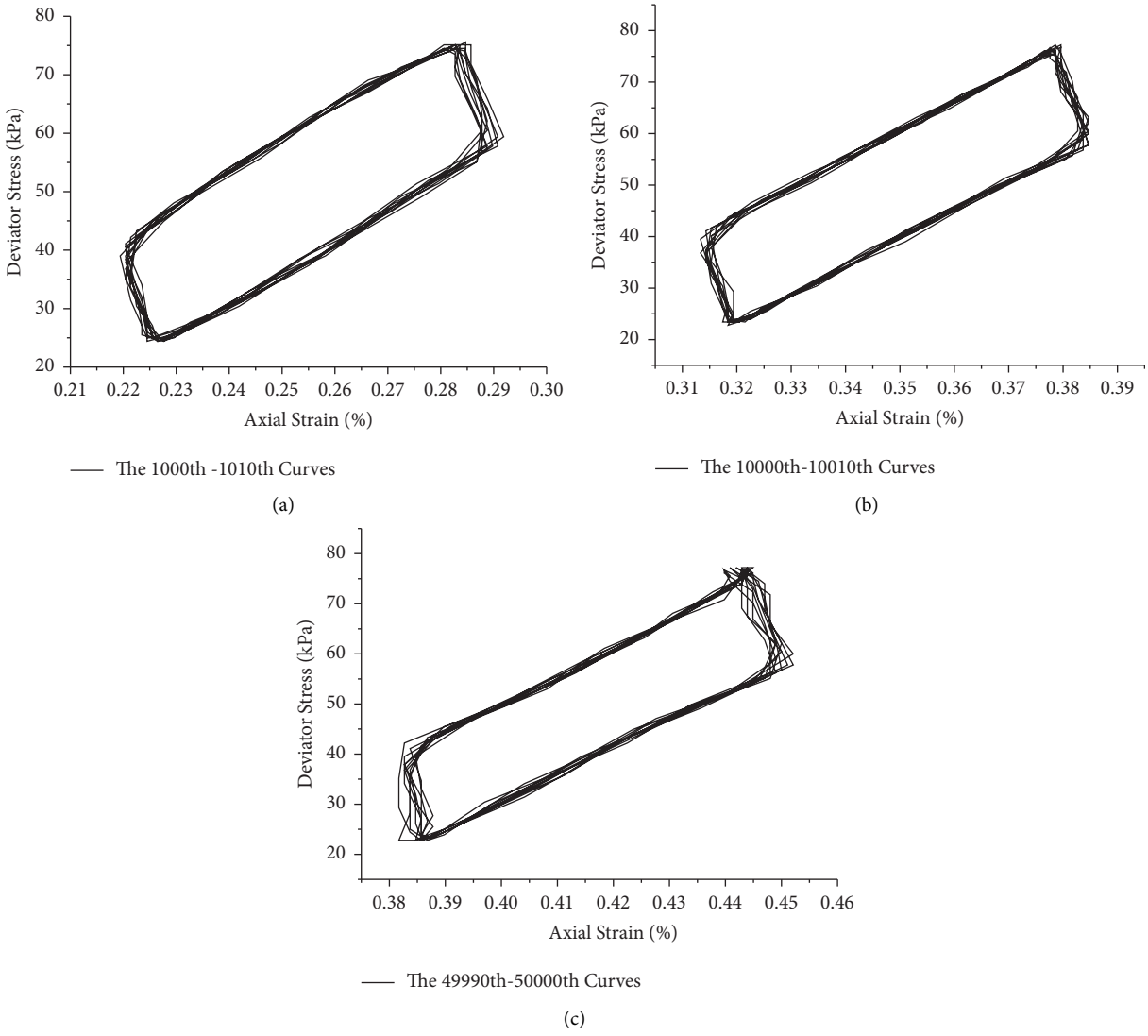


Figure 3: The hysteretic curves while $\sigma_3 = 25$ kPa, $|\sigma_1 - \sigma_3|_{max} = 75$ kPa. (a) The $1000^{th}$–$1010^{th}$ curves. (b) The $10000^{th}$–$10010^{th}$ curves. (c) The $49990^{th}$–$50000^{th}$ curves.

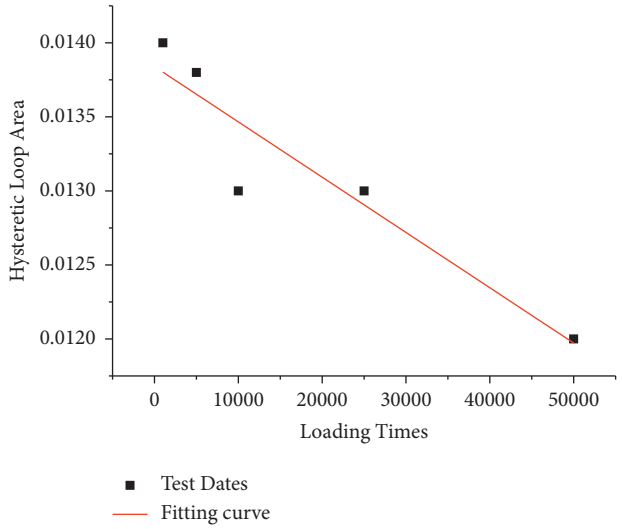


Figure 4: The relationship between hysteretic curve area and cycle times.

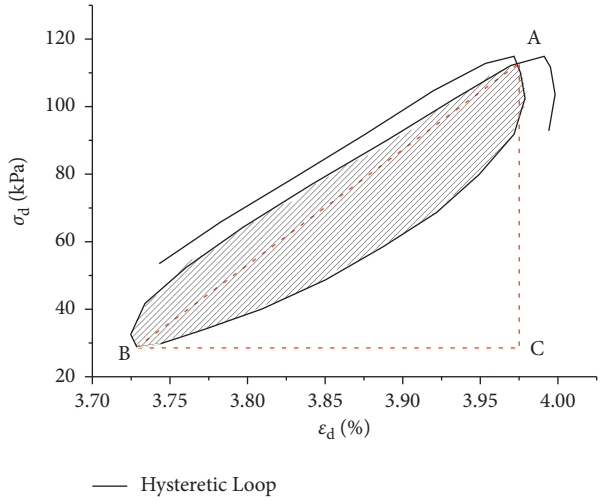


Figure 5: The hysteretic curve.

Table 2: The dynamic modulus and damping ratio.

| Loading times | 1000 | 5000 | 10000 | 25000 | 50000 |
|---|---|---|---|---|---|
| $E_d$/MPa | 90 | 90.9 | 86.4 | 93.8 | 96.1 |
| $\lambda$ | 0.33 | 0.29 | 0.26 | 0.26 | 0.25 |

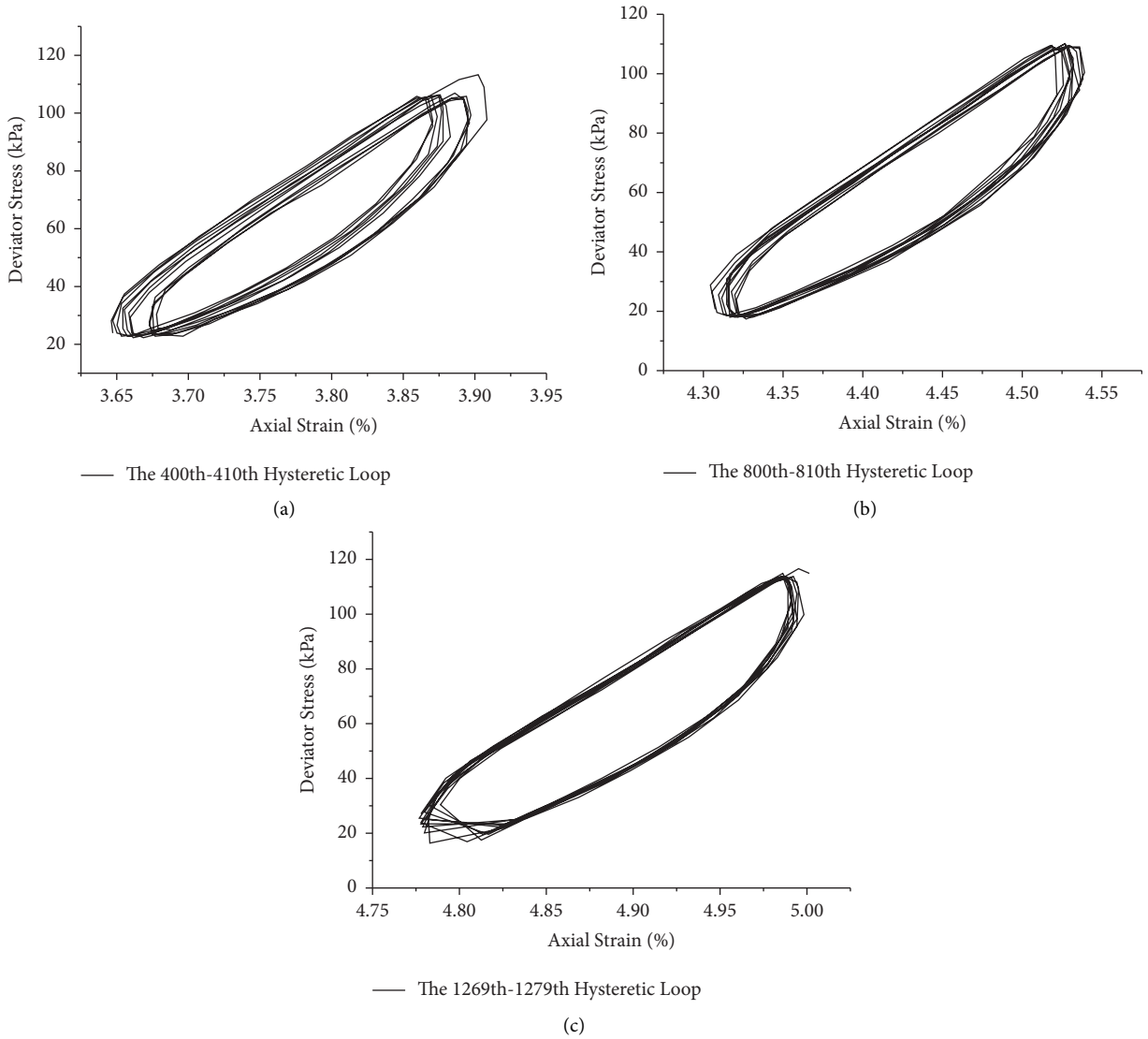


Figure 6: The hysteretic curves while $\sigma_3 = 20$ kPa, $|\sigma_1 - \sigma_3|_{max} = 100$ kPa. (a) The $400^{th}$–$410^{th}$ hysteretic loop curves. (b) The $800^{th}$–$810^{th}$ hysteretic loop curves. (c) The $1269^{th}$–$1279^{th}$ hysteretic loop curves.

When the cyclic loading time is 154, the axial strain reaches 5%, and then, the test was stopped. Extracting from the $50^{th}$, $75^{th}$, $100^{th}$, $125^{th}$, and $150^{th}$ hysteretic loops, the relationship between the loop area and loading time is shown in Figure 9.

The hysteretic loop area linearly decreases with loading time basically, and its value can be calculated by the following equation:

$$S = -1.0 \times 10^{-4} N + 0.0887, \quad (5)$$

where $N$ is the loading time. The correlation coefficient is above 0.98 for equation (5).

The dynamic modulus and damping ratio were gained from the $50^{th}$, $75^{th}$, $100^{th}$, $125^{th}$, and $150^{th}$ hysteretic loop curves and are listed in Table 4.

Both the dynamic modulus and damping ratio decrease with loading times basically, and the damage accumulation was always developing in this process until the sample failed.

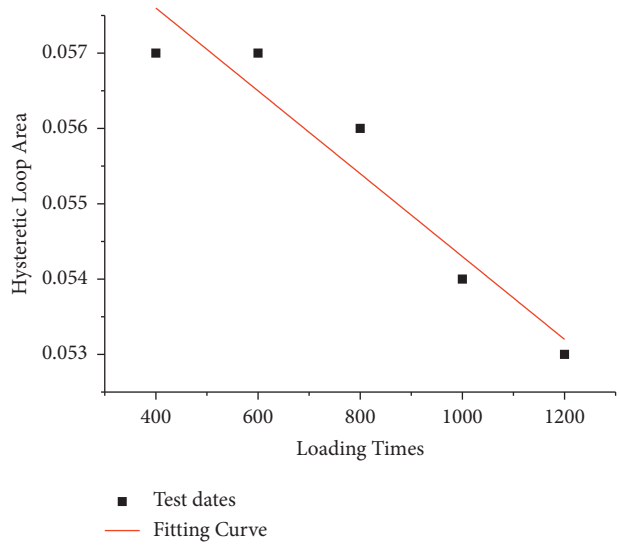


Figure 7: The relationship between hysteretic loop area and loading times.

Table 3: The dynamic modulus and damping ratio.

| Loading tines | 400 | 600 | 800 | 1000 | 1200 |
|---|---|---|---|---|---|
| $E_d$/MPa | 41.5 | 41.2 | 45 | 38.2 | 37.1 |
| $\lambda$ | 0.22 | 0.20 | 0.22 | 0.23 | 0.24 |

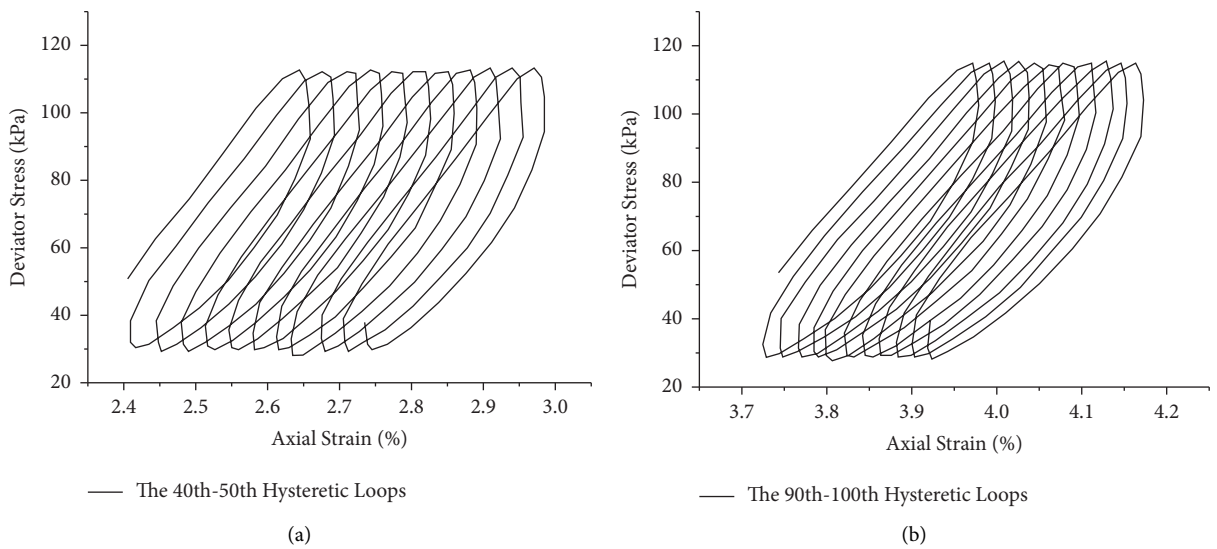


Figure 8: Continued.

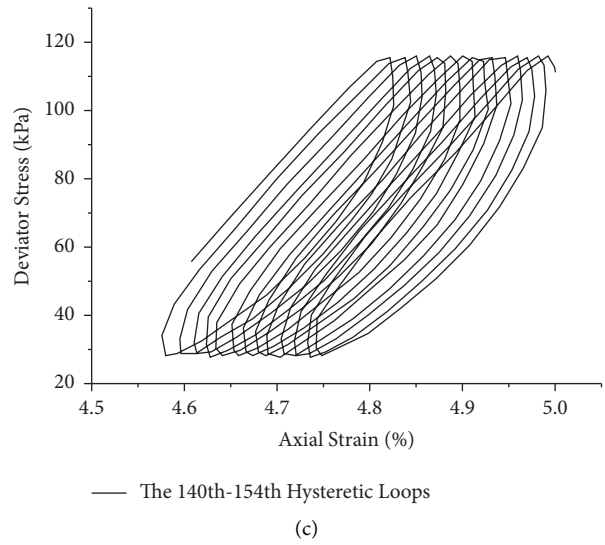


(c)

Figure 8: The hysteretic curves while $\sigma_3 = 30$ kPa, $|\sigma_1 - \sigma_3|_{max} = 115$ kPa. (a) The $40^{th}$–$50^{th}$ hysteretic loop curves. (b) The $90^{th}$–$100^{th}$ hysteretic loop curves. (c) The $140^{th}$–$154^{th}$ hysteretic loop curves.

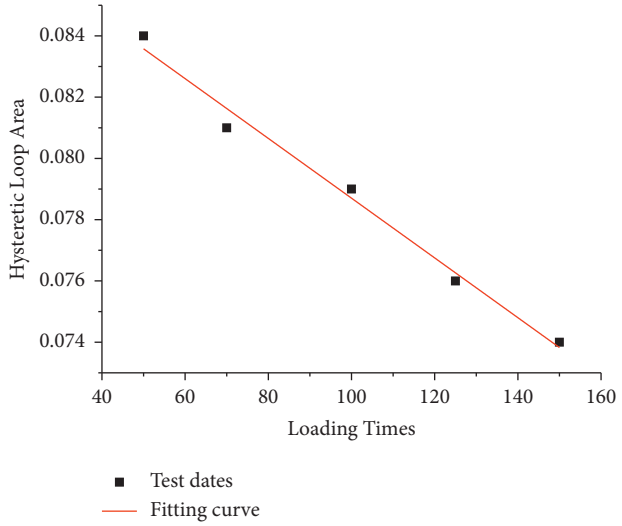


Figure 9: The relationship between hysteretic loop area and loading times.

Table 4: The dynamic modulus and damping ratio.

| Loading times | 50 | 75 | 100 | 125 | 150 |
|---|---|---|---|---|---|
| $E_d$/MPa | 36.9 | 35.1 | 36.3 | 35.7 | 33.6 |
| $\lambda$ | 0.28 | 0.25 | 0.24 | 0.23 | 0.23 |

## 4. Conclusion

Different deviator stress with 6 Hz is loaded on the specimens separately when the temperature is kept at −1.5°C, and the axial pressure is cyclic loading with different confining pressure and different amplitude. The results show that the mechanical properties of warm permafrost are related to the deviator stress. As the confining pressure and deviator stress amplitude are both 25 kPa, the hysteretic loops are approximately rectangular, and the specimen is always stable during the test process. When the confining pressure is 20 kPa and deviator stress amplitude is 40 kPa, the hysteretic loop curves become smother and appear oval. The specimen failed after 1279 loading times. With increasing deviator stress amplitude, the failed loading time declines rapidly. When the confining pressure is 30 kPa and deviator stress amplitude is 42.5 kPa, the specimen failed just after 154 loading times.

With the smallest deviator stress amplitude, the dynamic modulus increases slightly for the compression. When the deviator stress increases, the dynamic modulus decreases for the damage accumulation in other tests. The hysteretic loop area linearly decreases with loading time in all tests.

## Data Availability

The data used to support the findings of this study are included within the article.

## Conflicts of Interest

The authors declare that they have no conflicts of interest.

## Acknowledgments

This research was funded by the China State Construction Engineering Corporation (CSCEC-2020-Z-41).

## References

[1] S. W. Liu and J. M. Zhang, "Review on physic-mechanical properties of warm frozen soil," *Journal of Glaciology and Geocryology*, vol. 34, no. 1, pp. 120–129, 2012.

[2] C. H. Xu, X. Y. Xu, M. G. Qiu, X. Z. Li, and X. X. Chang, "Experimental study on dynamic damping ratio of frozen soil under cyclic loading," *Journal of Harbin University of C.E. & Architecture*, vol. 35, no. 6, pp. 22–25, 2002.

[3] S. P. Zhao, Y. L. Zhu, P. He, and D. Y. Wang, "Testing study on dynamic mechanics parameters of frozen soil," *Chinese Journal of Rock Mechanics and Engineering*, vol. 22, no. 2, pp. 2677–2681, 2003.

[4] Z. H. Gao and J. Shi, "Experimental study of the dynamic stength characteristics and residual strain of ice-rich frozen soil," *Journal of Glaciology and Geocryology*, vol. 31, no. 6, pp. 1143–1149, 2009.

[5] Z. H. Gao, Y. M. Lai, E. G. Xiong, and B. Li, "Experimental study of characteristics of warm and ice-rich frozen clay under cyclic loading," *Rock and Soil Mechanics*, vol. 31, no. 6, pp. 1744–1751, 2010.

[6] Y. H. Shi, P. He, and X. L. Bian, "Esting study on dynamic parameters of warm frozen soil of Qinghai-Tibet railway," *Subgrade Engineering*, vol. 128, pp. 93–95, 2006.

[7] F. Luo, S. P. Zhao, W. Ma, and G. D. Jiao, "Analysis of dynamic properties of frozen clay by morphological characteristics of hysteresis curves," *Rock and Soil Mechanics*, vol. 36, no. S1, pp. 299–304, 2015.

[8] S. J. Zhang, Y. M. Lai, S. Y. Li, and X. X. Chang, "Dynamic strength of frozen soils," *Chinese Journal of Geotechnical Engineering*, vol. 30, no. 4, pp. 595–599, 2008.

[9] J. K. Liu, Y. H. Cui, X. Liu, and D. Chang, "Dynamic characteristics of warm frozen soil under direct shear test-comparison with dynamic triaxial test," *Soil Dynamics and Earthquake Engineering*, vol. 133, pp. 106114–106212, 2020.

[10] F. He, X. Wang, D. R. Liu, D. J. Jiang, and B. S. Liu, "Experimental study on dynamic characteristic parameters of undisturbed frozen sandy soil of Qinghai-Tibet railway," *Journal of the China Railway Society*, vol. 39, no. 6, pp. 112–117, 2017.

[11] Y. Xue, J. Liu, P. G. Ranjith, Z. Zhang, F. Gao, and S. Wang, "Experimental investigation on the nonlinear characteristics of energy evolution and failure characteristics of coal under different gas pressures," *Bulletin of Engineering Geology and the Environment*, vol. 81, no. 1, pp. 38–26, 2022.

[12] Y. Xue, J. Liu, X. Liang, S. Wang, and Z. Ma, "Ecological risk assessment of soil and water loss by thermal enhanced methane recovery: numerical study using two-phase flow simulation," *Journal of Cleaner Production*, vol. 334, no. 1, Article ID 130183, 2022.

[13] X. J. Ma, J. M. Zhang, X. X. Chang, B. Zheng, and M. Y. Zhang, "Experimental study on creep of warm and ice-rich frozen soil," *Chinese Journal of Geotechnical Engineering*, vol. 29, no. 6, pp. 848–852, 2007.

[14] Y. Qin, J. Zhang, B. Zheng, and X. Ma, "Experimental study for the compressible behavior of warm and ice-rich frozen soil under the embankment of Qinghai–Tibet Railroad," *Cold Regions Science and Technology*, vol. 57, no. 2-3, pp. 148–153, 2009.

[15] B. Ladanyi, "Shallow foundations on frozen soil: creep settlement," *Journal of Geotechnical Engineering*, vol. 109, no. 11, pp. 1434–1448, 1983.

[16] T. Wang, G. Zhou, X. Jiang, and J. Wang, "Assessment for the spatial variation characteristics of uncertain thermal parameters for warm frozen soil," *Applied Thermal Engineering*, vol. 134, pp. 484–489, 2018.

[17] G. C. Sun, J. M. Zhang, Y. S. Dang, and C. Ding, "Microstructure and strength features of warm and ice-rich frozen soil treated with high-performance cements," *Journal of Mountain Science*, vol. 16, no. 6, pp. 1470–1482, 2019.

[18] M. Chai and J. Zhang, "Improvement of compressibility and thaw-settlement properties of warm and ice-rich frozen soil with cement and additives," *Materials*, vol. 12, no. 7, pp. 1068–1070, 2019.

[19] Z. Chen, X. X. Guo, L. T. Shao, S. Q. Li, and L. X. Gao, "Sensitivity analysis of the frozen soil nonlinear latent heat and its precise transformation method," *Geophysical Journal International*, vol. 228, no. 1, pp. 240–249, 2021.

[20] K. Hansson, J. Simunek, M. Mizoguchi, L. C. Lundin, and M. T. van Genuchten, "Water flow and heat transport in frozen soil: numerical solution and freeze-thaw applications," *Vadose Zone Journal*, vol. 3, no. 2, pp. 693–704, 2004.

[21] Q. Z. Li, Y. M. Lai, X. T. Xu, Y. G. Yang, and X. X. Chang, "Triaxial strength distribution of warm frozen soil and its damage statistical constitutive model," *Journal of Glaciology and Geocryology*, vol. 32, no. 6, pp. 1234–1241, 2010.

[22] M. Luetschg, M. Lehning, and W. Haeberli, "A sensitivity study of factors influencing warm/thin permafrost in the Swiss Alps," *Journal of Glaciology*, vol. 54, no. 187, pp. 696–704, 2008.

[23] Z. Wen, Y. Sheng, W. Ma, and J. Qi, "In situ experimental study on thermal protection effects of the insulation method on warm permafrost," *Cold Regions Science and Technology*, vol. 53, no. 3, pp. 369–381, 2008.

[24] B. Zheng, J. Zhang, and Y. Qin, "Investigation for the deformation of embankment underlain by warm and ice-rich permafrost," *Cold Regions Science and Technology*, vol. 60, no. 2, pp. 161–168, 2010.

[25] W. Ma, Z. Wen, Y. Sheng, Q. Wu, D. Wang, and W. Feng, "Remedying embankment thaw settlement in a warm permafrost region with thermosyphons and crushed rock revetment," *Canadian Geotechnical Journal*, vol. 49, no. 9, pp. 1005–1014, 2012.

[26] H. Jin and M. C. Brewer, "Highway roadway stability influenced by warm permafrost and seasonal frost action: a case study from glennallen, Alaska, USA," *Cold Regions Science and Technology*, vol. 1, pp. 26–41, 2008.

[27] G. Y. Li, N. Li, and W. Ma, "Cooling effects and mechanisms of crushed rock protective slopes combined with Shading board on embankment in warm permafrost regions," *Rock and Soil Mechanics*, vol. 31, no. 1, pp. 165–173, 2010.

[28] Q. Zhang, N. Li, W. Ma, Y. H. Mu, and G. Y. Li, "Analyses of the thawing consolidation of fill embankments in warm permafrost regions," *Journal of Glaciology and Geocryology*, vol. 36, no. 3, pp. 614–621, 2014.

[29] L. D. Shields, H. Fensury, and R. Kenyon, "The deformation properties of warm underocean permafrost," *Civil Engineering in the Arctic Offshore ASCE*, pp. 593–603, 1985.

[30] Y. Qin and J. Zhang, "Estimating the stability of unprotected embankment in warm and ice-rich permafrost region," *Cold Regions Science and Technology*, vol. 61, no. 1, pp. 65–71, 2010.

[31] T. Gb, *Code for Measurement Methods of Dynamic Properties of Subsoil*, China Planning Press, Beijing, China, 2016.